Journal of Nuclear Materials 392 (2009) 405–412

Contents lists available at ScienceDirect

Journal of Nuclear Materials

journal homepage: www.elsevier.com/locate/jnucmat

Liquid metal corrosion/erosion investigations of structure materials in lead cooled systems: Part 1

M. Kieser *, H. Muscher, A. Weisenburger, A. Heinzel, G. Müller

Forschungszentrum Karlsruhe GmbH, Institut für Hochleistungsimpuls und Mikrowellentechnik, Hermann-von-Helmholtz-Platz 1, 76344 Eggenstein-Leopoldshafen, Germany

ARTICLE INFO

Article history:
Received 10 April 2008
Accepted 22 December 2008

PACS:
C09
L03
S06

ABSTRACT

In future lead cooled nuclear power systems the heavy liquid-metal pump will be placed in the hot temperature region of the reactor. This combines corrosion problematic at elevated temperatures with erosion at the impeller of the pump. Several steels designed for conventional mechanical high loaded pumps and the SiSiC have been tested in oxygen containing stagnant lead (10^{-6} and 10^{-8} wt%) at 550 and 600 °C for 2000 and 4000 h in the COSTA-facilities. Only SiSiC shows no influence by the liquid metal. No dissolution attack occurs at cast iron steels but inner oxidation takes place. NORILOY shows no dissolution attack. All other steels are attacked by liquid lead at one of the conditions. To evaluate the erosion–corrosion attack a new test facility allowing velocities of the lead of up to 20 m/s was designed and constructed. With a CFD-code the behaviour and flow velocity of the lead are simulated.

1. Introduction

In the both main design concepts concerning transmutation of minor actinides, GEN IV and/or the ADS, the coolant has to be transported and circulated just in the same manner as in conventional nuclear power systems [1–5]. The thermo-physical properties of liquid metals (LM) with low melting and high boiling temperatures, like the alkali metals with small atomic weight and heavy liquid metals like lead or its alloys, makes them attractive as coolant candidates in advanced nuclear fusion and fission systems. The fast neutron spectrum and the high neutron yield of the spallation reaction enable simple and robust flow structures with high energy densities. Thus, liquid metals are attractive for the development of neutron spallation sources, for fusion blankets, as core coolant of fast reactors and for heavy ion fragmentation experiments. However, the practical use of LM still needs to be demonstrated by experiments and by numerical predictions. One of the main problems in the development of such a system is compatibility of the steels with LM. Corrosion effects in the 100 μm range are reported on ferritic Fe–Cr steels between 575 and 750 °C after 3250 h exposure to liquid lead [6]. Steel components are soluble in liquid lead in the range of 10^{-3}–0.1 at.% in this temperature region [7]. An exception exists for Ni, which has a solubility of 2 at.% at 600 °C in lead [8]. The dissolution of steel components weakens the steel structure which can lead to heavy corrosion effects with high flow velocities.

In general the countermeasure against dissolution of steel components by liquid lead alloys is formation of a protective oxide scale on the steel surface which is stabilized by oxygen dissolved in the liquid alloy. This method was extensively studied and described very recently [9]. The oxide scale hinders cation diffusion from the steel into the liquid metal and vice versa.

In future liquid metal cooled nuclear power systems it is discussed to place the heavy liquid-metal pump in the thermally hot part of the reactor. This combines the known corrosion problematic at elevated temperatures with expected erosion at the impeller of the pump. The present paper describes the behaviour of steels which are used for convectional pumps and the ceramic material SiSiC in stagnant lead at 550 and 600 °C up to 4000 h by an oxygen concentration of 10^{-6} and 10^{-8} wt% in the liquid lead. In the second part of this paper the design and construction of a facility for combined corrosion erosion test of the materials is described. A CFD-code is used to simulate the flow conditions (velocities at each of the specimens exposed) in this new test facility.

2. Experimental

2.1. Materials tested

The compositions of the steels and the SiSiC ceramic used in the experiments are given in Table 1. The specimens are plates of $28 \times 8 \times 2$ mm^3 dimension.

All steels employed were selected from the pump material port folio of KSB Company and delivered by them. The ceramic composite (SiSiC) applied by KSB in sea water desalination pumps as bearing for extreme high loaded regions was provided by Schunk

* Corresponding author. Tel.: +49 7247 82 8475; fax: +49 7247 82 2256.
E-mail address: martin.kieser@ihm.fzk.de (M. Kieser).

0022-3115/$ - see front matter © 2009 Published by Elsevier B.V.
doi:10.1016/j.jnucmat.2008.12.327

Table 1
Chemical composition of the materials tested in stagnant lead.

Description/trade name	Chemical composition in wt%						
	C	Si	Mn	Cr	Ni	Mo	Cu
NORIHARD®	2.6	0.6	0.7	15		2.6	
NORILOY®	1.7	⩽1	⩽1	25		2.0	
Chrome cast iron	⩽0.1	⩽1	⩽1	13	1.5	⩽0.5	
Martensitic cast iron	⩽0.06	⩽1	⩽1	13	4	⩽0.7	
NORIDUR®	⩽0.04	⩽1.5	⩽1.5	25	6	2.5	3.0
NORICID®	⩽0.04	⩽4.5	⩽4.5	20	13	0.2	
SiSiC							

Ingenieurkeramik, Corp. As a rule, the reaction-bonded silicium enriched silicon carbide (SiSiC) consists of approximately 85–94% of SiC and correspondingly from 15% to 6% semimetallic silicon. SiSiC has virtually no residual porosity. This is achieved by filling the matrix of silicon carbide crystals with additional silicon infiltrated. The reaction between liquid silicon and the carbon leads to a SiC-binding matrix, the rest of the pore space is filled with excess silicon. The advantage of this special manufacturing technology is that unlike other SiC powder interaction techniques, the components during the process exhibit nearly no shrinkage. Therefore, very large components can be manufactured with precise dimensions. The use of SiSiC is limited due to the melting point of silicon to about 1400 °C. Up to this temperature range, SiSiC possess high strength and resistance towards corrosion and erosion, combined with good thermal shock resistance and wear resistance. SiSiC is therefore recommended as a material for highly loaded parts such as various components of burner for direct and indirect combustion (for example nozzles). SiSiC ceramics is also used in other mechanical engineering devices as well as corrosion-resistant parts (seals, pump blades) of high wear.

Selection of the steels was performed considering variations of the element content (Table 1). Two Ni free steels differing in Cr. Two cast iron steels differing in Ni and high Cr Ni steels with different Ni-content and one with relatively high Si share.

2.2. Exposure facility (COSTA) and experimental condition

The experiments are conducted in the COSTA device [10] in which the specimens are exposed to stagnant lead under defined and controlled temperature and oxygen concentration conditions. The control of oxygen concentrations is obtained in this device via the gas phase by establishing the corresponding oxygen partial pressure via the H_2/H_2O ratio in the gas flowing through the furnace tubes [11]. All specimens were exposed in liquid lead with oxygen concentration of 10^{-6} and 10^{-8} wt% at temperatures of 550 and 600 °C. Two test runs with 2000 and 4000 h duration were conducted. The test conditions represent two different regimes: at 10^{-6} wt% Fe-oxides are thermodynamically stable; at 10^{-8} wt% the oxygen activity is too low to form these Fe-oxides. In the stable regime (10^{-6} wt%) a magnetite and wustite scale develop on the surface by diffusion of iron into this scale and subsequent oxidation [12]. At the lower oxygen-content magnetite and wustite are not stable any more. However, in Fe–Cr steels with more than 3 wt% a Cr-spinel of type $Fe(Fe_{1-x}Cr_x)_2O_4$ develops below the surface by diffusion of oxygen [10,13]. When the Cr-content exceeds 8 wt% [14] – like in the materials described in this paper – both spinel formation and FeO formation is observed in low oxygen conditions. With the help of tracer diffusion measurements it is shown by Töpfer et al. [15] that the Fe ion diffusion coefficient decreases by up to two orders of magnitude with increasing Cr-content in the spinel for low oxygen activities in which the diffusion is governed by cation interstitials.

2.3. Experiment's evaluation

The specimens taken out of the COSTA device after the experiments are cut using a diamond disk saw perpendicular to the exposed surface and are grinded and polished for metallographic examinations. Light optical (LOM) and scanning electron (SEM) microscopy (S-800, Hitachi) are employed for observation of the microstructure of the material and the oxide scale. The identification of the phases is supported by energy dispersive X-ray analysis (EDX, WINEDS Thomson Scientific).

3. Results and discussion after exposure in stagnant liquid lead

3.1. Nickel free steels: NORIHARD® and NORILOY®

The effect of lead on NORIHARD after 4000 h at two temperatures and 10^{-6} wt% oxygen concentration in the liquid metal is shown in Fig. 1. At 550 °C a non-uniform oxide layer is formed, Fig. 1 left. Thin Cr-oxide or thicker Cr–Fe-spinel layers, both covered with magnetite, protect the steel. NORIHARD and NORILOY have a two phase structure varying in Cr concentration. The nature of the oxide scale depends on the Cr concentration of the grain at the surface. At higher Cr-contents thin Cr-oxide scale at lower Cr-content Cr-spinel layers are formed.

Such a non-uniform oxide layer was already observed at 600 °C after 2000 h. After 4000 h a severe dissolution attack with penetration depths of more than 70 μm is depicted in Fig. 1 right. The bright lines are lead inclusions embedded in the steel matrix.

Fig. 2 shows the cross section of the specimens after 4000 h exposure at 550 and 600 °C in liquid lead containing 10^{-8} wt% oxy-

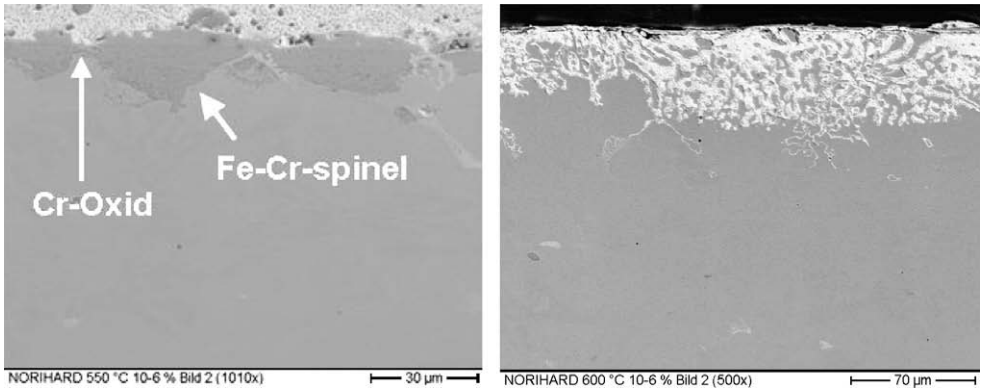

Fig. 1. SEM cross section of NORIHARD® after 4000 h exposure with 10^{-6} wt% oxygen in lead. Left: a thin Cr-oxide or Cr–Fe-spinel scale covered with magnetite protects the steel at 550 °C. Right: a severe dissolution attack occurred at 600 °C.

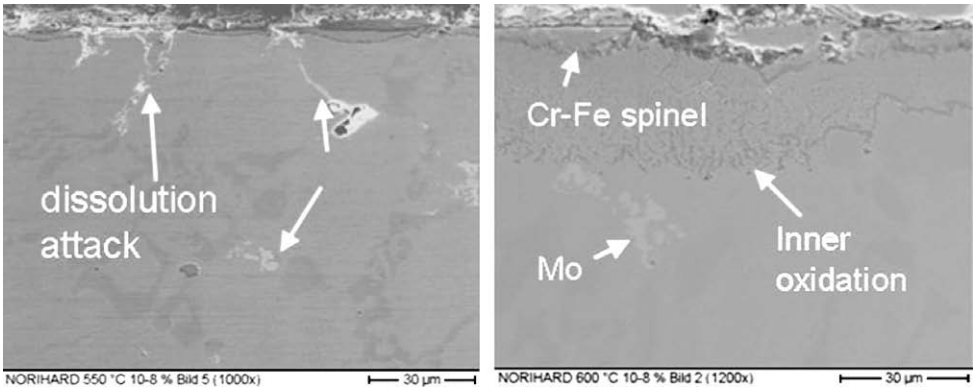

Fig. 2. SEM cross section of NORIHARD® after 4000 h exposure at 550 °C (left) and 600 °C (right) and 10^{-8} wt% O.

gen. At 550 °C, Fig. 2 left side, most part of the surface is protected by a thin Cr-oxide or Fe–Cr-spinel layer. Below the spinel layer at the border to the bulk material a Cr-rich band appears. Very local dissolution attack with 30 µm deep penetration of lead into the steel is observed. The other brighter spots in the bulk are Mo inclusions. The specimen exposed at 600 °C, Fig. 2 right, shows an extended inner oxidation zone that is not observed on the 550 °C specimen. At 600 °C the entire surface is protected by a Cr–Fe-spinel that is not sealed against oxygen diffusion. The diffused oxygen forms Cr-rich oxides along the grain boundaries. The inner oxidation zone has a maximum thickness of 25 µm.

The corrosion behaviour of NORILOY in lead is similar to that of NORIHARD, apart that at all temperatures non-uniform oxide layer of Cr-oxide or Fe–Cr-oxide protects the surface, see Fig. 3. No dissolution attack is observed at all conditions. The frequency of Fe–Cr-spinel scales is significant lower compared to the NORIHARD, mainly due to the overall higher Cr-content of the steel.

3.2. Chromium cast iron and martensitic cast iron

Both steels show similar behaviour in liquid lead. The steels are mostly protected by a Fe–Cr-spinel or Cr-oxide with inner oxidation growing by time and temperature. The thickness of the formed spinel and inner diffusion zone is depicted in Table 2. The oxide layers grown on the martensitic cast iron are always thicker compared to scales formed on the Cr–cast iron steels.

Fig. 4 shows the behaviour of the Cr–cast iron after 4000 h exposure at 550 and 600 °C and 10^{-6} wt% oxygen (top)/10^{-8} wt% oxygen (below) in lead. At 10^{-6} wt% oxygen at both temperatures, Fig. 4 above, no dissolution attack is visible, but some parts of the spinel layer spall off. Therefore the oxide layer is wavy, Fig. 4, right above. Such spallation was not observed at the martensitic cast iron. Only at one condition, 550 °C and 10^{-8} wt% the Cr–cast iron grows a thin protective Cr-oxide scale not visible at Fig. 4 left below. At a temperature of 600 °C with same oxygen-content an

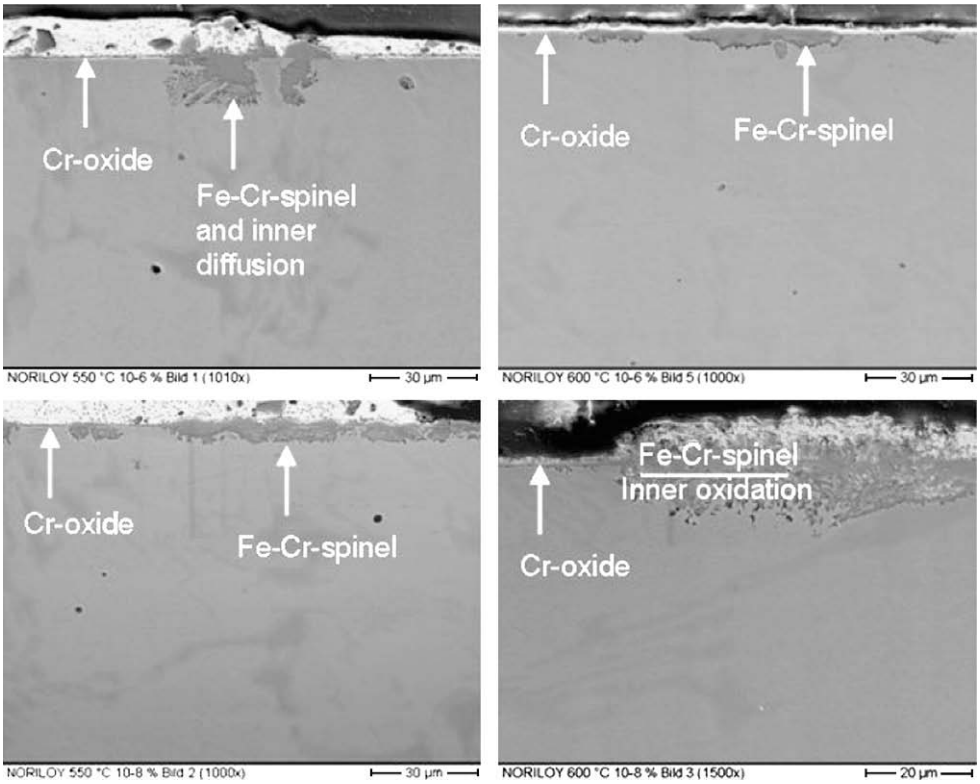

Fig. 3. SEM cross section of NORILOY® after 4000 h exposure at 550 and 600 °C and 10^{-6} wt% (top)/10^{-8} wt% (below) oxygen in lead. All specimens are protected by a non-uniform oxide layer consisting of Cr-oxide or Fe–Cr-spinel.

Table 2
Measurement of the oxide thickness in μm at Cr– and martensitic cast iron after 4000 h.

		10^{-6} wt% 4000 h (μm)	10^{-8} wt% 4000 h (μm)
Chromium cast iron	550 °C	16–17	<1
	600 °C	~12	~11
Martensitic cast iron	550 °C	16–17	~10
	600 °C	~21	~21

11 μm thick inner oxidation zone could be observed. There contrary to the specimens exposed at 10^{-6} wt% oxygen no Fe–Cr-spinel layer formed on top of the steel could be observed.

3.3. High Cr Ni steels: NORIDUR® and NORICID®

NORIDUR® and NORICID® have both 25 wt% Cr but different Ni-contents. NORICID® contains in addition 4.5 wt% Si which is known to improve the corrosion resistance.

Fig. 5 shows the SEM cross sections of NORIDUR® after 4000 h exposure at 10^{-6} wt% oxygen in the lead. At 550 °C, Fig. 5 left, a thin non-visible oxide layer protects the steel during the whole exposure time. At the higher temperature the steel was only protected up to 2000 h after 4000 h, Fig. 5 right, a severe LM dissolution attack occurs. The bright spots are lead that penetrates up to 70 μm deep into the steel matrix. In this area Ni and Cr is entirely leached out. Such strong dissolution attack is observed at all specimens exposed in lead containing 10^{-8} wt% oxygen at both temperatures already after 2000 h.

NORICID® forms in lead containing 10^{-6} wt% oxygen at both temperatures thick layered oxide scales. A Cr–Si-rich oxide is interrupted by almost pure metallic iron, Fig. 6. Such oxidation is similar to inner oxidation horizontal to the surface. At 550 °C the scales grow to a thickness of about 20 μm. At 600 °C the scale of about the same thickness spalls off at most of the surface, Fig. 6 right. However, under these conditions, the Si does not form a protective thin Si-oxide scale. At 550 °C and 10^{-8} wt% oxygen the oxide layer formed after 2000 h spalls off after 4000 h. Specimens exposed to lead at 600 °C and 10^{-8} wt% oxygen show severe dissolution attack already after 2000 h.

3.4. Composite material SiSiC

The best behaviour of all tested materials shows the composite SiSiC: No LM attack no extensive oxidation layer was observed in all experiments, Fig. 7. Under stagnant conditions this material is entirely unaffected by the liquid lead. The porosity depicted in the near surface regions is also seen in the unexposed samples, Fig. 7 left. Therefore, to simplify the post-examination, specimens will be polished before applying them in the erosion test facility.

4. The erosion test facility

The main demand by developing the erosion test stand was the simulation of the relative velocities between the samples and the HLM under defined conditions regarding oxygen concentration and temperature [16]. In general it is a two container concept, one container – for conditioning the liquid lead, the other – to perform the erosion tests.

4.1. Experimental setup

The photograph of the facility's interior (Fig. 8) is showing some details of its engineering design: parts of the magnetic agitator as well as the body of the rotating inner cylinder. The entire facility is designed for tests in lead having a temperature up to 650 °C and oxygen concentrations from 10^{-10} to 10^{-4} wt%. To ensure such

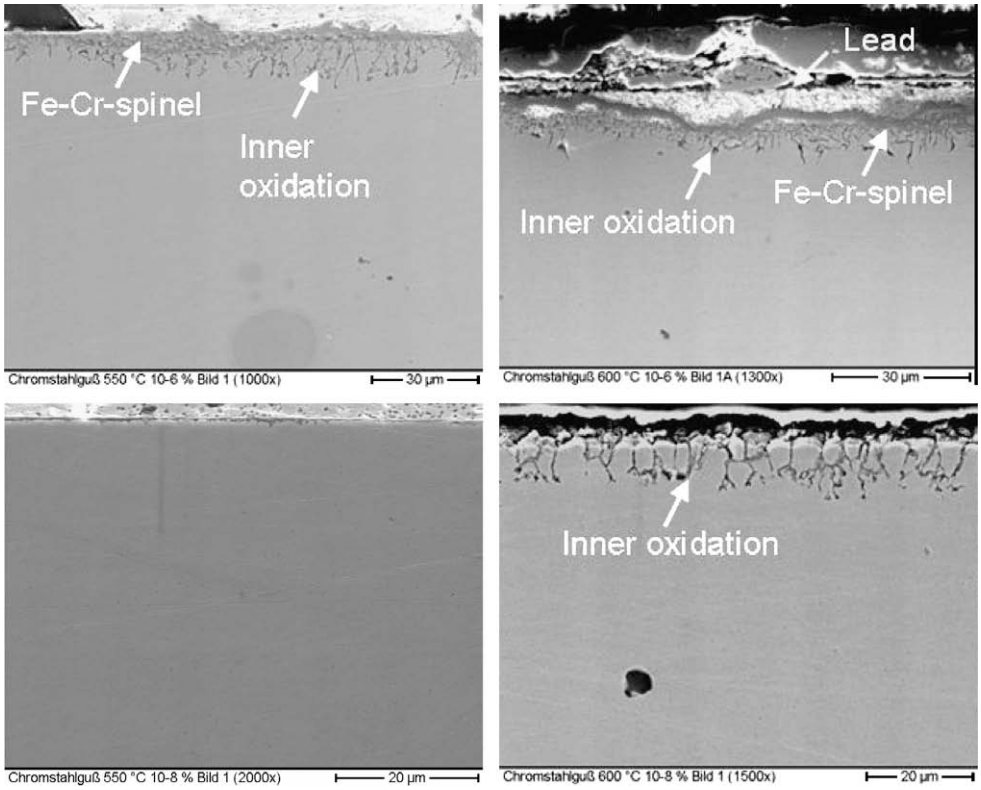

Fig. 4. SEM cross section of chromium cast iron after 4000 h exposure at 550 and 600 °C and 10^{-6} wt% (top)/10^{-8} wt% oxygen in lead (below).

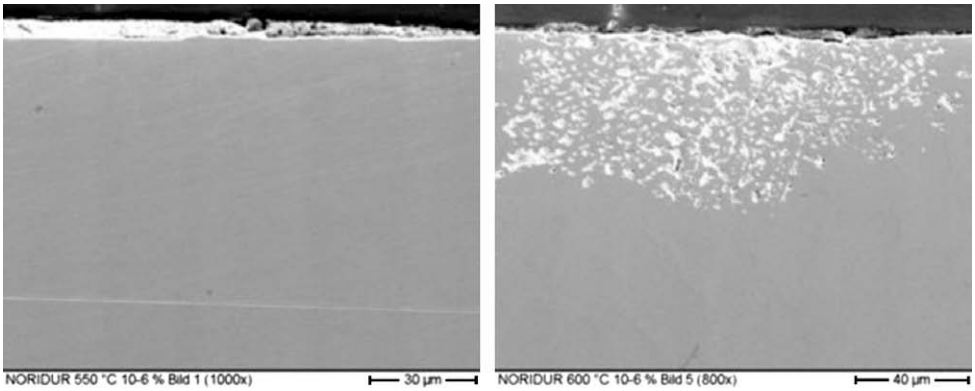

Fig. 5. SEM cross section of NORIDUR® after 4000 h exposure in 10^{-6} wt% O containing lead. Left: at 550 °C a thin not visible oxide layer protects the steel; right: at 600 °C a severe LM dissolution attack occurs.

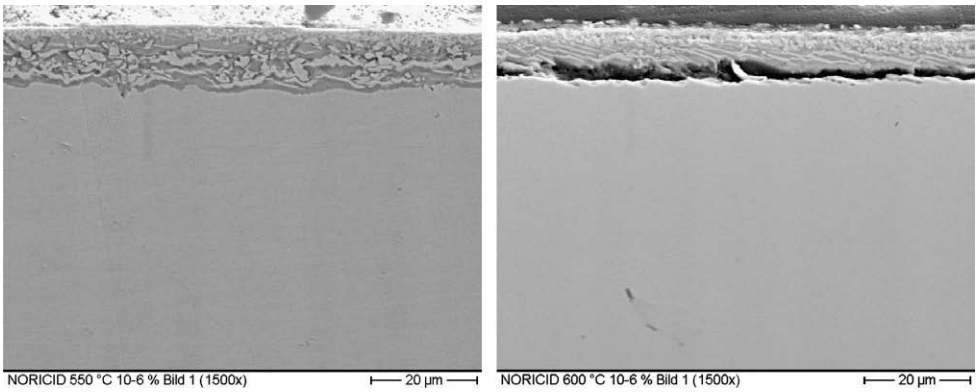

Fig. 6. SEM cross section of NORICID® after 4000 h exposure in 10^{-6} wt% O containing lead. Left: at 550 °C thick layered oxide layer protects the steel; right: at 600 °C oxide layer spallation.

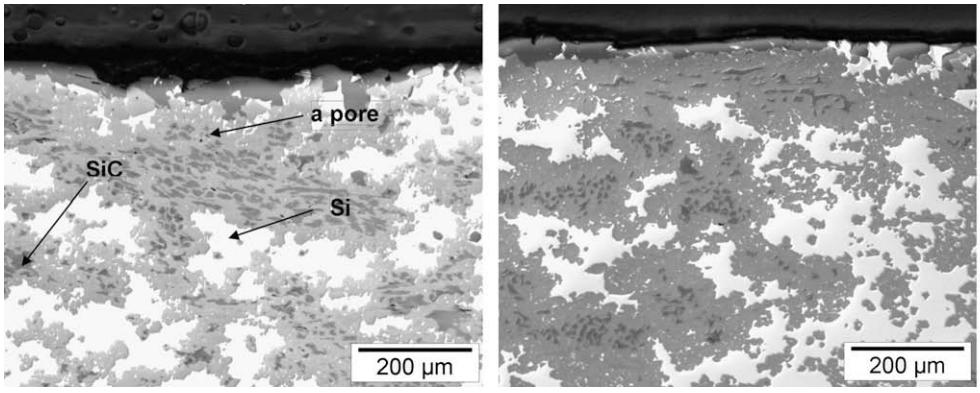

Fig. 7. Cross section of SiSiC. Left unexposed specimen; right: specimen exposed at 600 °C, 10^{-8} wt% oxygen.

stringent conditions the facility has to be absolutely gas-tight. The most critical part is the transfer of the rotation speed into the experimental container.

To avoid any sealing problems a magnetic coupling was designed and constructed. The major challenge for this coupling was the high temperature in the facility. Most of the permanent magnets have a Curie-temperature below the envisaged temperatures. The magnets chosen were AlNiCo 500 delivered from IBS Company in Berlin. Twenty four magnets in the outer and inner rotating cylinder guarantee a rotation speed of up to 2000 rpm of the inner cylinder. The lead that is accelerated by the inner cylinder (Fig. 8) will develop a velocity profile that can be calculated roughly as given by the formula (Eq. (1)):

$$U_\phi = \frac{\omega_1 R_1^2}{R_2^2 - R_1^2}\left(\frac{R_2^2 - r^2}{r}\right), \tag{1}$$

where ω_1 is the angular rotation speed of the inner cylinder, R_2 – the inner diameter of the container and R_1 – the outer diameter of the rotating inner cylinder [17].

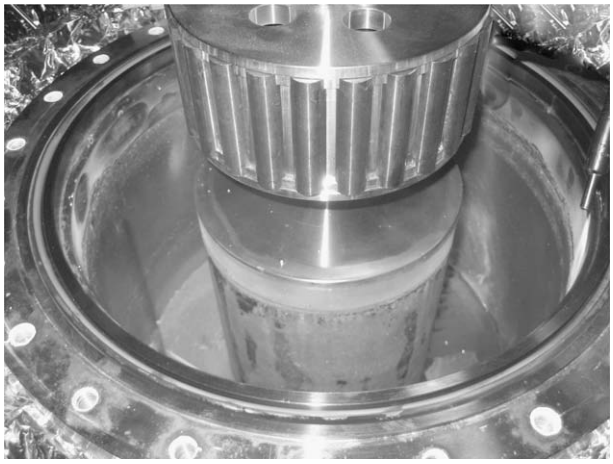

Fig. 8. Photograph of the erosion test stand's interior showing parts of the magnetic agitator and the rotating inner cylinder.

The test facility is equipped with an automatic oxygen control system (OCS) that measures and controls the oxygen partial pressure in the gas mixture. Doing so, the oxygen activities in the liquid lead are controlled, too [11]. Temperature, the EMF data corresponding to the oxygen level in the lead as well as the flow velocities are measured and stored by a data acquisition system. The conditioning of the lead is performed in the conditioning container. A stirrer – magnetic coupled and rotating with about 60 rpm – is installed to accelerate the oxygen transport into the volume of the liquid. The lead will be transferred via a stainless steel tube connecting both containers. The tube can be heated to allow the transfer of the conditioned lead and can be cooled to block the transfer by freezing the lead in the tube. Heating of the containers is realized by heating rods bended around each container and a heating plate placed below each. This allows a precise control of the temperature in the containers. The containers are isolated with the purpose to minimize heat losses and improving the homogeneity of the temperature distribution in the liquid lead, within limits of about ±0.5°, see Fig. 9.

The dimensions of the facility are the following: outer diameter of the containers: exact 320 mm, diameter of the inner cylinder – 159 mm, height of the containers 220 mm, volume of lead ca. 15 dm^3, which provides to a filling level of about 60%.

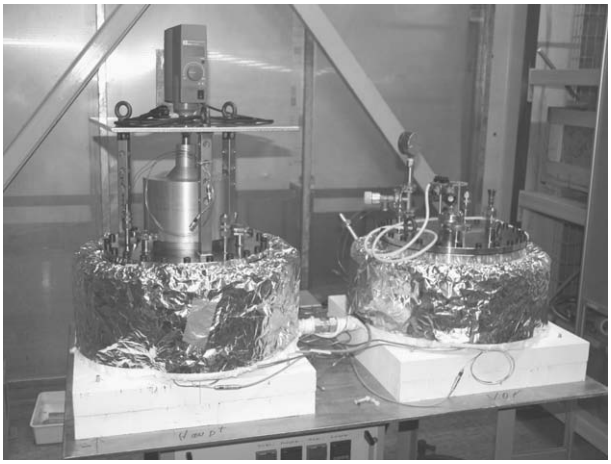

Fig. 9. Photograph of the test facility, the conditioning chamber on the right part, the experimental container on the left part.

The LM corrosion/erosion experiments will be performed in the following way. The test specimens, equal flat plates of $60 \times 15 \times 1.5$ mm^3, are placed in the experimental container and the container itself is evacuated and purged using the gas atmosphere necessary for the required oxygen levels. At first the lead is conditioned in the right chamber (Fig. 9) to achieve the defined temperature and the oxygen concentration requested. After reaching the preset values (measured using a Pt/air–oxygen sensor placed in the lead) the transfer tube is heated up and the lead is transferred into the experimental container (Fig. 9, left side). The transfer tube is cooled down and the frozen lead seals the connection between conditioning and experimental container. After freezing of the lead remaining in the transfer tube the experiment starts. The duration will be between 500 and 2000 h with specimens not being pre-exposed. Additional experiments with pre-exposed specimens will be performed, too.

One uncertainty is the relative velocity of the liquid lead and the test specimen. The specimens can be placed symmetrically but at different radial positions to test in one run different relative lead velocities. The measurement of the flow velocity (Pitot-tube method) will be performed only at one position, however. Therefore modelling the flow characteristics is fundamental for interpretation of the test results.

4.2. CFD modelling of the flows in the erosion test stand without obstacles

The geometry of the specimens flat planar plates offer several advantages for the simulation of the experiment [18] and for the design and the performance of the experiments itself. However, the chosen geometry is not only of theoretical importance because components with planar geometries are often used in various technical devices e.g. turbine blades and in other applications of practical relevance.

Analyzing the flow generated by the rotating lateral surface of the inner cylinder as well as the horizontal basal disk [19,20], one should take into account the obvious need, to minimize, for the seek of simplicity, the 'end–edge-effects' – by appropriate manufacturing, i.e. 'rounding' the sharp edges between the disk and the lateral cylindrical surface to simplify the geometry of the inner rotating cylinder. Doing so, the flow can 'tranquilize' to some extend, resulting in a smoother transition between both the lateral and the horizontal induced flows. The intensive parameters (p, T) are chosen as $T = 600$ °C and $p = 1$ bar. The fluid is assumed to be incompressible and viscous. At first, the flow of the liquid metal is regarded as laminar. (The flow in the gas phase above the liquid metal remains turbulent.) LM-calculations are performed with respect to the wetted part of the steel plates interface only. The CFD software tool that is chosen for the simulation is the multiphysics package *fluidyn 5.1*.

Fluid dynamic modelling always starts with the defining of geometries as well as generation of meshes. The *fluidyn* CADGEN does not support CAD CATIA files directly. However, the corresponding ∗.igs format can be exported by CATIA geometry/mesh creator. Such an IGES file containing also the specimens is shown in Fig. 10. IGES files can be imported and converted to a ∗.NEU neutral, unstructured file by a *fluidyn* interface. After that procedure, some mesh grids of different types have been done on IGES geometries. The methodology here was to mesh the pre-assigned ∗.iges geometries with CADGEN.

Local refinement of the mesh in the regions of the steel sheet is an obvious need. This is in accordance with the appropriate wall modelling. Grid refinement at boundaries near the flow obstacles can be done with the help of defined (special) stretching functions via the command line of the *fluidyn* interface. Generally spoken, arbitrary mesh coupling and grid refinement at interfaces itself

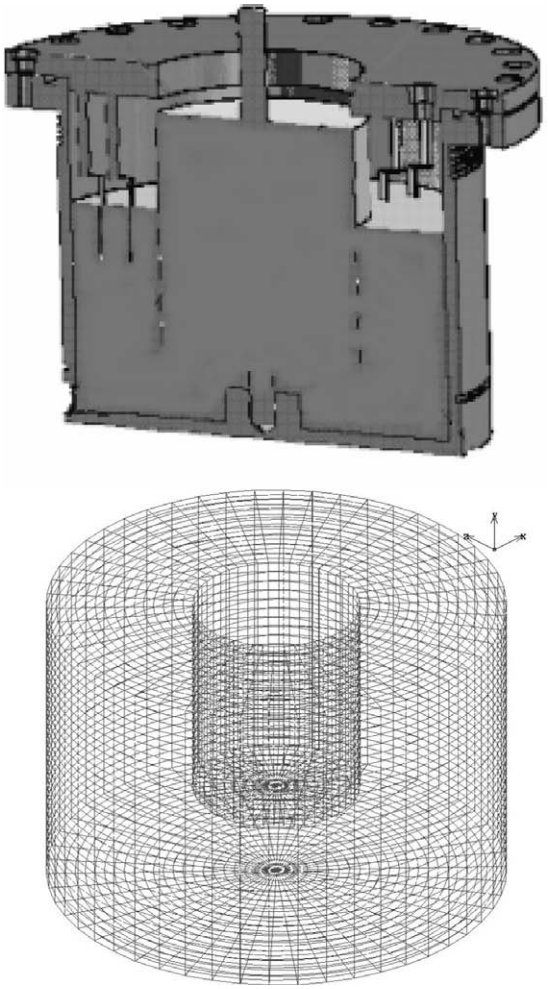

Fig. 10. Left: IGES file of experimental container needed for the mesh generation; right: meshed experimental container.

or extended changes of element types in the critical regions of high flow gradients have to be avoided. The assumptions made when setting up the grid with regard to critical regions of high flow gradients and large changes have to be compared with the first (draft) results of the computation, and grid points are to be rearranged if it is found to be necessary. It can happen that the fastest way to mesh, the CCDT Delaunay triangularisation, is not the best choice and the cases can be launched only in tetrahedral mesh. The final meshing of the lead in the experimental arrangement is depicted in Fig. 10 right.

As a first attempt to the real simulation the flow velocities as a function of the radial position are calculated. Boundary conditions for this calculation a speed of the inner cylinder of 4.5 m/s. The overall flow profile looks very close to the simplified analytic calculation (Eq. (1)). The major differences are the more rapid drop of the velocity near the inner rotating cylinder (Fig. 11 left). Preliminary simulation of the free surface flow-profiles at the interface lead/gas (Ar and Ar–5%H_2 mixture) was done using the volume of fluid tool (VoF) in *fluidyn* multiphysics, the volume-of-fluid method, led to a graphical representation shown in Fig. 11 right. The expected free surface profile is clearly visualised as a result of proper modelling, NS-simulation and the final graphical post-processing. Further simulation of the (u, v, w)-flow velocities in the gap between two concentric cylinders (inner rough wall rotating, several obstacles) will consider the measurement at defined position using the Pitot tube and adapting the CFD model to match the simulation with the measured values for verification and validation purposes.

5. Conclusions and outlook

The use of a rotating cylinder facility operating under controlled fluid dynamic conditions is of interest for tests of the combined corrosion–erosion (LMC/LME) behaviour of possible pump materials in lead cooled reactors.

Several in other industrial fields applied pump materials have been tested in stagnant lead at relevant conditions. One steel, Noriloy with a Cr-content of 25 wt% shows at all conditions promising compatibility with lead. All other steels show either dissolution or severe oxidation at least under one selected condition, and this even at stagnant conditions. The best behaviour of all tested materials was exhibited by the SiSiC composite material.

Beside Noridur, Norihard and Noricid all other materials will be tested under combined erosion–corrosion dynamic conditions in the designed facility. The test stand is taken into operation and first results will be available soon. The relative velocity at each sample position will be calculated applying the CFD-codes of *fluidyn*. Meshing procedures of the test arrangement and first preliminary Navier Stokes-calculations are performed. The final simulation will

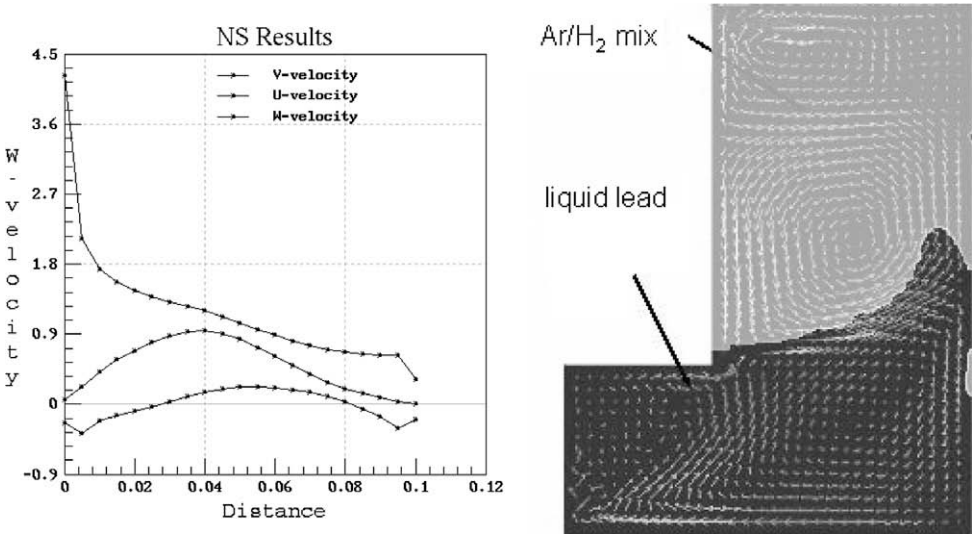

Fig. 11. Flow velocities (left) and free surface two phase boundary (right).

consider the flow velocity measured over a long time at a single defined point.

Acknowledgements

We like to thank the KSB Stiftung for their financial support and providing the test structure materials and the Director S. Tripathi as well as Dr J. Hamburger, both *transoft France*, for software assistance while setting up the cases.

References

[1] G.M. Tolson, A. Taboada, A Study of Lead and Lead-Salt Corrosion in Thermal Convection Loops, AEC Accession No. 23603, Rept. No. ORNL-TM-1437, Oak Ridge Natl. Lab., Oak Ridge, TN, 1966, 18.
[2] A.J. Romano, C.J. Klamut, D.H. Gurinsky, The Investigation of Container Materials for Bi and Pb Alloys, Part I, Thermal Convection Loops, BNL 811 (T-313), 1963.
[3] G. Benamati, C. Fazio, H. Piankova, A. Rusanov, J. Nucl. Mater. 301 (2002) 23.
[4] I.V. Gorynin, G.P. Karzov, V. Markov, V.S. Lavruchin, V.A. Yakovlev, in: Proceedings Conference HLMC 98, vol. 1, SSC RF – IPPE, Obninsk, 1999, p. 120.
[5] J. Zhang, N. Li, Y. Chen, A.E. Rusanov, J. Nucl. Mater. 336 (2005) 1.
[6] G.Y. Lai, High Temperature Corrosion of Engineering Alloys, ASM Int., Materials Park, OH, 1990.
[7] R.P. Elliott, Constitution of Binary Alloys, First Supplement, McGraw-Hill, 1965.
[8] T. B. Massalski (Ed.), Landolt-Börnstein, New Series IV, 5, 1995.
[9] B.F. Gromov, Yu.I. Orlov, P.N. Martynov, K.D. Ivanov, V.A. Gulevski, in: H.U. Borgstedt, G. Frees (Eds.), Liquid Metal Systems, Plenum, New York, 1995, p. 339.
[10] G. Müller, G. Schumacher, F. Zimmermann, J. Nucl. Mater. 278 (2000) 85.
[11] G. Müller, A. Heinzel, G. Schumacher, A. Weisenburger, J. Nucl. Mater. 321 (2003) 256.
[12] K. Hauffe, Oxidation of Metals, Plenum, New York, 1965.
[13] T. Furukawa, K. Aoto, G. Müller, G. Schumacher, A. Weisenburger, A. Heinzel, F. Zimmermann, J. Nucl. Sci. Technol. 41 (3) (2004) 265.
[14] A.S. Khanna, High Temperature Oxidation and Corrosion, ASM Int., 2002.
[15] J. Töpfer, S. Aggarwal, R. Dieckmann, Solid State Ionics 81 (1995) 251.
[16] F. Balbaud-Célérier, F. Barbier, J. Nucl. Mater. 289 (2001) 227.
[17] F.M. White, Viscous Fluid Flow, second ed., McGraw-Hill Int., 1991.
[18] M. Schäfer, Computational Engineering, Springer, Berlin, 2006.
[19] H. Schlichting, Grenzschicht – Theorie, Verlag G. Braun, Karlsruhe, 1965.
[20] V.G. Levich, Physicochemical Hydrodynamics, Prentice Hall, Inc., NJ, 1962.